Effect of rare-earth ion Ho substitution on the structural, optical, and electrical properties of Mg-doped Cd-Co ferrites

M. I. Arshad [a], Ihab M. Moussa[b], N. Amin [a], S. Mumtaz [c], Z. Munir [a], M. R. Saleem [a], M.S. Hasan [d,*]

[a]*Department of Physics, Government College University, Faisalabad 38000, Pakistan*

[b]*Department of Botany and Microbiology, College of Science, King Saud University, P.O. Box 2455, Riyadh, 11451, Saudi Arabia*

[c]*Department of Electrical and Biological Physics, Kwangwoon University, Seoul 01897, South Korea*

[d]*Institute of Functional Nano & Soft Materials (FUNSOM), Jiangsu Key Laboratory for Carbon-Based Functional Materials & Devices, Soochow University, Suzhou, China*

Coprecipitation method was used to create a sequence of $Cd_{0.6}Mg_{0.4}Fe_{1.9}Ho_{0.1}O_4$ and $Cd_{0.6}Mg_{0.2}Co_{0.2}Fe_{1.9}Ho_{0.1}O_4$ soft ferrites. The structural, optical, and electrical characteristics were assessed using the XRD, FTIR, UV-vis, and four probe I-V methods, respectively. XRD pattern verified the cubic crystal structure. For both kinds of samples, the average crystallite size was between 23.2 and 25.6 nm. The presence of the tetrahedral band was demonstrated by FTIR spectra. As the percentage of Co^{2+} increased, Eg was found to be 2.70 eV and 2.57 eV. DC electrical resistivity values of 5.01 x 10^6 and 1.26 x 10^7 ohm-cm proved that synthesized samples may be utilised in transformers to reduce their eddy current losses.

(Received November 15, 2024; Accepted January 28, 2025)

Keywords: Soft ferrites, Coprecipitation, Optical bandgap energy, FTIR, DC resistivity

1. Introduction

The exceptional optical, magnetic, and electrical properties of soft ferrites have made them suitable for use in a wide range of devices [1-8]. The general molecular formula for soft magnetic oxides is $[A][B_2]O_4$, here [A] represents a divalent cation, such as Co^{2+}, Zn^{2+}, Mg^{2+}, Cd^{2+}, or Ni^{2+} and [B] represents the trivalent ions like Fe^{3+} and rare earth metals (La^{3+}, Y^{3+}. Sm^{3+}, Ce^{3+}, Ho^{3+} etc.) In the face-centered cubic (FCC) lattice structure of spinel, the bivalents and Fe^{3+} ions reside at the tetrahedral [A] and octahedral [B] interstitial sites, respectively, with oxygen ions forming the regular spinel lattice [9-11]. $MgFe_2O_4$ and $CoFe_2O_4$ both exhibit an inverse spinel structure. Nevertheless, they have a mixed spinel structure when the crystallite size is lowered to the nanometre domain and they had lower magnetic moment values at low temperatures respect to bulk materials [12, 13]. Changes in the coordination of cation of A-sites and B-sites or the redistribution of cations are thought to be the cause of this transition from inverted to mixed spinel structures. Consequently, in the $MgFe_2O_4$ and $CoFe_2O_4$ structures, Mg, Co, and Fe^{3+} ions occupy both A and B interstitial positions [14]. Catalysis, ferrofluids, microwaves, gas sensors, medical technologies, optics, and magnetic devices are just a few of the sectors in which these soft ferrites find use [15, 16].

Co^{2+} (ferromagnetic) ions are used in place of Mg^{2+} (paramagnetic) ions in the current study, and $Cd2^{+}$ is also added to the mixture. Cd^{2+}, which has a normal spinel configuration, occupies the tetrahedral site [A]. To enhance the magnetic properties of the composition, Co^{2+} ions are substituted for Mg^{2+} ions. Holmium (Ho), known for its paramagnetic nature, occupies the

* Corresponding author: m.sajjadhasan@hotmail.com
https://doi.org/10.15251/DJNB.2025.201.121

octahedral B-site, and has a reversed spinel configuration. To further enhance the magnetic properties, a precise quantity of Ho is added. Co^{2+}-doped $Cd_{0.6}Mg_{0.4-x}Co_xFe_{1.9}Ho_{0.1}O_4$ (x = 0.0 and 0.2) [*CMHF and CMCHF soft ferrites*] nanoparticles have not yet been described, according to an in-depth review of the literature. Numerous techniques, including sol-gel auto ignition, co-precipitation, hydrothermal, green synthesis spray pyrolysis, and microwave refluxing, may be used to create these ferrite nanoparticles [17-19]. In this research, co-precipitation was chosen as the synthesis method due to its cost-effectiveness and widespread use in achieving the desired results [20-22]. In current study we have synthesised the Co^{2+} doped *CMHF and CMCHF soft ferrites* where, x = 0.0 and 0.2. The structural, optical, and electrical characteristics of the constructed ferrites are examine using X-ray diffraction, FTIR-spectroscopy, UV-Vis, and current-voltage measurement.

2. Synthesis and characterizations

The co-precipitation method for synthesizing $Cd_{0.6}Mg_{0.4-x}Co_xFe_{1.9}Ho_{0.1}O_4$ (x = 0.0 and 0.2) involves dissolving stoichiometric amounts of Cd^{2+}, Mg^{2+}, Co^{2+}, Fe^{3+}, and Ho^{3+} salts in deionized water to form a homogeneous solution. A precipitating agent, such as sodium hydroxide (NaOH), is then added dropwise to the solution under constant stirring at 80 ℃ to achieve a pH of around 10-11, leading to the formation of a precipitates by placing the samples in preheated water bath. The precipitates were washed, filtered, and dried before being calcined at a high temperature (800 ℃) to form the desired ferrite nanoparticles. This process ensures controlled particle size and uniform composition. The structural, optical, and electrical characteristics of the nanomaterials were studied by using a variety of characterisation tools, such as FTIR spectroscopy, XRD, UV-vis, and current-voltage two probe methods.

3. XRD analysis

The XRD plot of synthesized samples *CMHF and CMCHF soft ferrites* are presented in Figure 1. Both samples exhibited a single-phase crystalline structure, with prominent peaks observed at (220), (311), (400), (422), and (511). Scherrer's equation [23] was used to determine the average value of crystallite size.

$$D = \frac{0.9\lambda}{\beta cos\theta} \tag{1}$$

Here, FWHM represents the full width at half maximum, and λ is the wavelength, taken as 1.542 Å for the Bragg angle. The calculated crystallite sizes are presented in Table 1. The lattice parameter, dislocation line density and unit cell volume [24] were determined using the corresponding equation.

$$a = d\sqrt{h^2 + k^2 + l^2} \tag{2}$$

$$V = a^3 \tag{3}$$

The correlation between average crystallite size D and lattice constant (lattice parameter) a with respect to Co^{2+} contents is seen in Fig. 2. The graph shows that as the concents of Co^{2+} grows, so does the average crystallite size. The lattice parameter appears to increase with higher Co^{2+} concentration and the fact is attributed to the replacement of Mg^{2+} (0.72 Å) with higher radii Co^{2+} (0.78 Å). This suggests that as Co^{2+} replaces Mg^{2+}, the lattice parameter expands because of the larger ionic radius of Co^{2+} compared to Mg^{2+} [25]. Table 1 also shows the trends for volume which is depending on the lattice constant values for both types of samples.

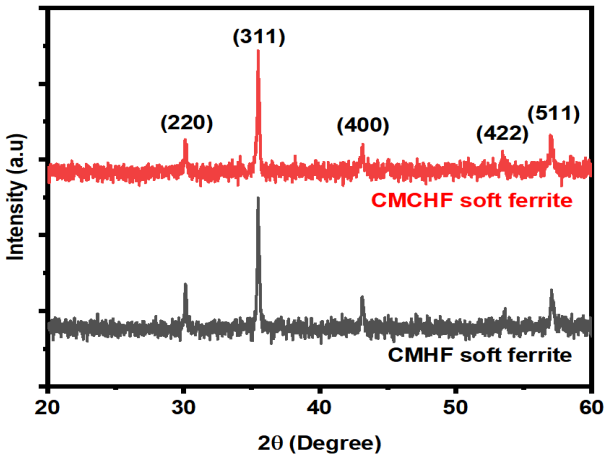

Fig. 1. XRD patterns for CMHF and CMCHF soft ferrites.

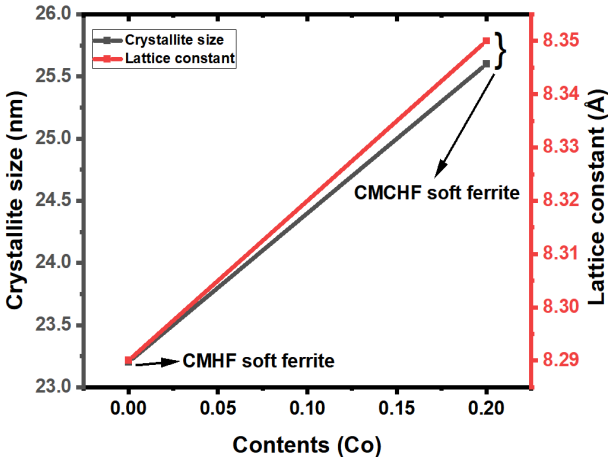

Fig. 2. Average crystallite size and lattice constant vs. cobalt concentration for CMHF and CMCHF soft ferrites.

Table 1. Compositional formula, diffraction angle (2θ), average crystallite size (D), lattice constant (a) and volumes (V) for CMHF and CMCHF soft ferrites.

Composition	2θ (Degree)	D (nm)	a (Å)	V $(Å)^3$
$Cd_{0.6}Mg_{0.4}Fe_{1.9}Ho_{0.1}O_4$	35.48	23.2	8.29	569.7
$Cd_{0.6}Mg_{0.2}Co_{0.2}Fe_{1.9}Ho_{0.1}O_4$	35.49	25.6	8.35	582.1

4. FTIR Analysis

FTIR spectroscopy was used to examine the arrangement of ions on tetrahedral and octahedral sites. Fig. 3 (a and b) shows the FTIR spectra for soft ferrites with compositions *CMHF and CMCHF soft ferrites*. The oxygen tetrahedron and Fe-O stretching vibrations are linked to the high-frequency band (ν_1). $Fe^{3+}(A/B)O_2^-$ vibrations, which are characteristic of spinel ferrite structures with a maximum valency of +3, belong to this frequency range. For x = 0.0 to 0.6, the ν_1 frequency bands range from 526.5 cm^{-1} to 535.8 cm^{-1}. Variations in the bond lengths between Fe^{3+} and O^{2-} at the tetrahedral site are believed to cause these shifts in band positions [26].

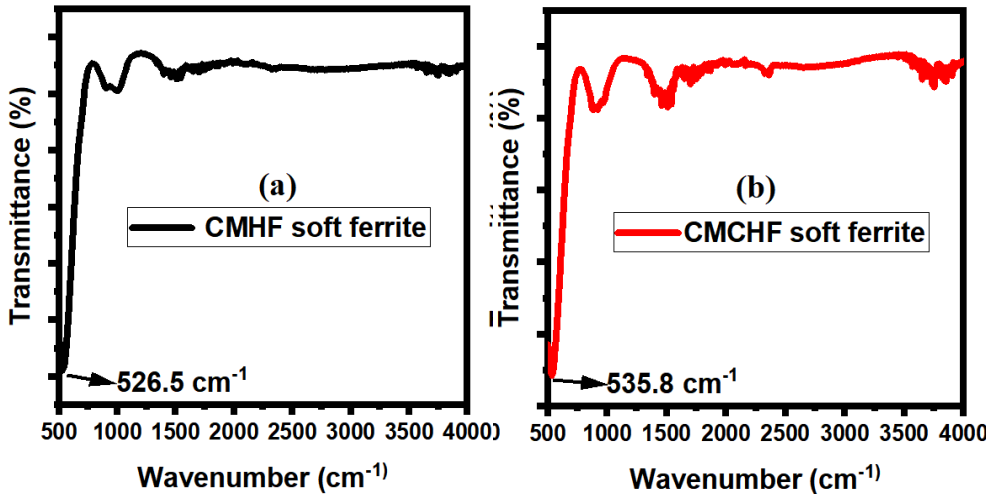

Fig. 3. (a & b). FTIR spectra of CMHF and CMCHF spinel ferrites.

Table 2. Tetrahedral bands, E_g and ρ_{DC} for CMHF and CMCHF soft ferrites.

Compositions	Tetrahedral band (cm^{-1})	E_g (eV)	ρ_{DC} (Ω cm)
$Cd_{0.6}Mg_{0.4}Fe_{1.9}Ho_{0.1}O_4$	526.5	2.70	5.01 x 10^6
$Cd_{0.6}Mg_{0.2}Co_{0.2}Fe_{1.9}Ho_{0.1}O_4$	535.8	2.57	1.26 10^7

5. UV-visible spectroscopy

A helpful method for determining the optical band gap energy of *CMHF and CMCHF soft ferrites* is UV-visible photometry. The equation below was used to get the absorption coefficient (α) [27]:

$$\alpha = 2.303\frac{logA}{t} \tag{4}$$

where, absorbance is denoted by A and thickness of sample holding cuvette by t. The optical energy band gap is then determined using Tauc's equation and is provided by [28]:

$$\alpha h\nu = B(h\nu - Eg)^m \tag{5}$$

where, v is the frequency, B is the transition probability constant, h is Plank's constant, and m is the number of absorption transition events. Plotting hν versus $(\alpha h\nu)^2$ yields the optical energy band gap, as depicted in Fig. 4. The optical energy band gap may be estimated by drawing a tangent to the x-axis. The calculated optical energy band gap is given in Table 2. According to the results, the optical band gap energy rises as the percentage of Co^2 ions grows. The level of dopant ions, the presence of impurities, or surface effects might all be responsible for this behaviour. Furthermore, the range of Eg indicates that the materials that were synthesised are appropriate for application in microwave frequency devices [14].

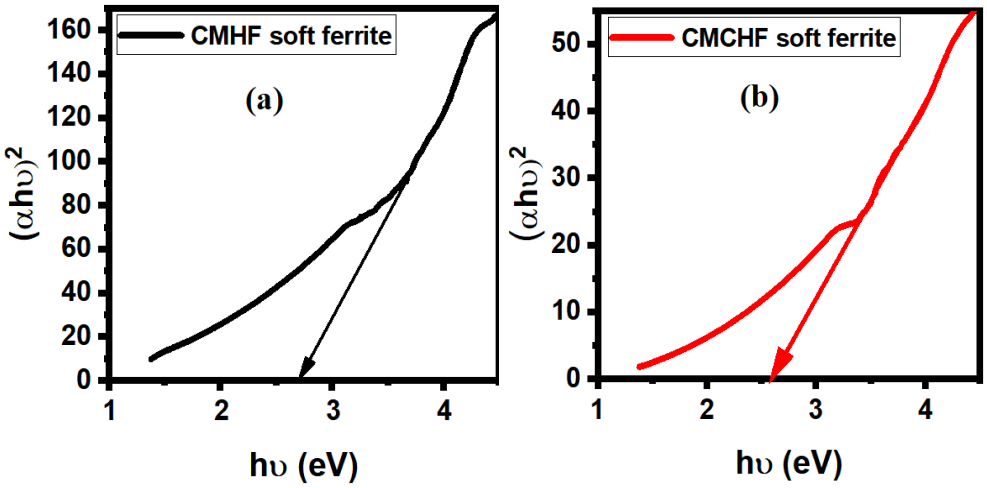

Fig. 4. (a & b). Optical bandgap energies for CMHF and CMCHF soft ferrites.

6. DC electrical resistivities

At room temperature, the DC electrical resistivity of *CMHF and CMCHF soft ferrites* was measured using the two probes approach. The DC resistivity of synthesized ferrites was determined using a relation is [29, 30]:

$$R = \frac{\rho L}{A} \tag{6}$$

where L and A stand for the thickness and area of the pellets, respectively. One may determine the resistance R by taking the inverse of slope obtained from IV graph. For *CMHF and CMCHF soft ferrites*, the DC electrical resistivity was 5.01 x 10^6 and 1.26 x 10^7 ohm-cm, respectively, as indicated in Table 2. The DC resistivity vs concentration curve is shown in Fig. 5. The graph shows how resistivity increases in tandem with the concentration of Co^{2+}. Charge carriers hopping is the cause of this phenomenon. Charge carrier hopping is the cause of this behaviour. Moreover, Mg^{2+} has a conductivity of 2.15 x 10^7 S/m, whereas Co^{2+} has a conductivity of 1.7 x 107 S/m. Therefore, the conduction process results of charge carriers hopping among trivalent and divalent iron ions. Therefore, when Co^{2+} ions are added, the conduction process decreases and the resistance increases [13].

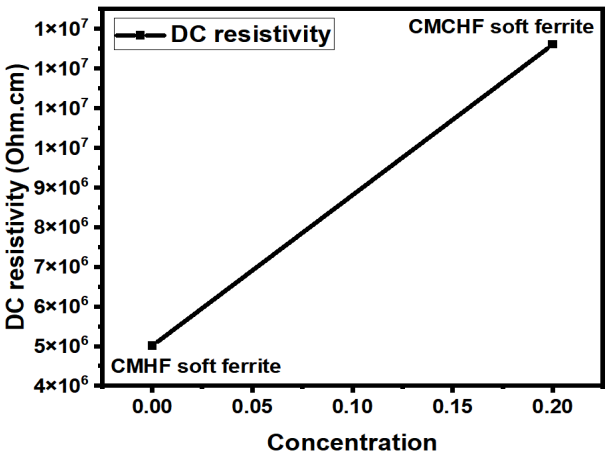

Fig. 5. DC resistivity for CMHF and CMCHF soft ferrites.

Conclusion

The series of Co^{2+} substituted $Cd_{0.6}Mg_{0.4-x}Co_xFe_{1.9}Ho_{0.1}O_4$ *ferrites* for (x = 0.0 and 0.2) were synthesized by co-precipitation process. XRD patterns confirmed the formation of spinel ferrites and confirmed that Co^{2+} has successfully entered into crystalline structure. Lattice constants increased from 8.29 Å to 8.35 Å with increase in Co^{2+} concentration. FTIR spectra showed the existence of tetrahedral bands. I-V analysis showed increase in resistivity from 5.01 x 10^6 ohm .cm and 1.26 x 10^7 ohm-cm. Increase in resistivity making these ferrites promising for use at high frequencies.

Funding

Researchers supporting project number (RSPD2025R741), King Saud University.

Acknowledgement

The authors would like to thank the Researchers Supporting Project number (RSPD2025R741), King Saud University, Riyadh, Saudi Arabia.

References

[1] Arshad, M., et al., Journal of Alloys and Compounds, 2024. 972: p. 172847; https://doi.org/10.1016/j.jallcom.2023.172847

[2] Arshad, M.I., et al., Powder Technology, 2024. 438: p. 119469; https://doi.org/10.1016/j.powtec.2024.119469

[3] Arslan, M., et al., Journal of Molecular Structure, 2024. 1318: p. 139237; https://doi.org/10.1016/j.molstruc.2024.139237

[4] Fatima, M., et al., ACS omega, 2023. 8(44): p. 41169-41181; https://doi.org/10.1021/acsomega.3c03993

[5] Hasan, M., et al., Journal of Alloys and Compounds, 2023. 956: p. 170392.

[6] Hasan, M., et al., Materials Science and Engineering: B, 2024. 301: p. 117180; https://doi.org/10.1016/j.mseb.2024.117180

[7] Hasan, M., et al., Ceramics International, 2024. 50(2): p. 3129-3138; https://doi.org/10.1016/j.ceramint.2023.11.062

[8] Hasan, M., et al., Inorganic Chemistry Communications, 2024. 167: p. 112666; https://doi.org/10.1016/j.inoche.2024.112666

[9] Akhtar, M., et al., Journal of Rare Earths, 2024. 42(1): p. 137-146; https://doi.org/10.1016/j.jre.2023.01.021

[10] Hasan, M., et al., Materials Chemistry and Physics, 2023. 301: p. 127538; https://doi.org/10.1016/j.matchemphys.2023.127538

[11] Mujtaba, A., et al., Journal of Materials Research and Technology, 2023. 23: p. 4538-4550; https://doi.org/10.1016/j.jmrt.2023.02.038

[12] Farooq, W.A., et al., Molecules, 2021. 26(5): p. 1399.

[13] Hasan, M., et al., Digest J. Nanomater. Biostruct, 2022. 17: p. 1527-1533.

[14] Arshad, M.I., et al., Ceramics International, 2022. 48(10): p. 14246-14260; https://doi.org/10.1016/j.ceramint.2022.01.313

[15] Nabi, M.A.U., et al., 2021. 34: p. 1813-1822; https://doi.org/10.1007/s10948-020-05588-x

[16] Zulqarnain, M., et al., Journal of Alloys and Compounds, 2022. 894: p. 162431; https://doi.org/10.1016/j.jallcom.2021.162431

[17] Amin, N., et al., Ceramics International, 2020. 46(13): p. 20798-20809; https://doi.org/10.1016/j.ceramint.2020.05.079

[18] Khan, M., et al., Ceramics International, 2020. 46(17): p. 27318-27325; https://doi.org/10.1016/j.ceramint.2020.07.217

[19] Saqib, M., et al., Journal of Superconductivity and Novel Magnetism, 2021. 34: p. 609-616; https://doi.org/10.1007/s10948-020-05746-1

[20] Amin, N., et al., Digest Journal of Nanomaterials and Biostructures. vol, 2019. 14: p. 501-507.

[21] Hasan, M., et al., Materials Research Express, 2018. 6(1): p. 016302; https://doi.org/10.1088/2053-1591/aae3f6

[22] Hussain, K., et al., Digest Journal of Nanomaterials and Biostructures. vol, 2019. 14: p. 85-92.

[23] Khan, M., et al., Physica B: Condensed Matter, 2024. 674: p. 415575; https://doi.org/10.1016/j.physb.2023.415575

[24] Nabi, M., et al., Dig. J. Nanomaterials Biostructures, 2018. 13: p. 1111-1116.

[25] Sarmah, S., et al., Ceramics International, 2023. 49(1): p. 1444-1463; https://doi.org/10.1016/j.ceramint.2022.09.126

[26] Sujatha, C., et al., Journal of magnetism and magnetic materials, 2013. 340: p. 38-45; https://doi.org/10.1016/j.jmmm.2013.03.027

[27] Khan, M., et al., Results in Chemistry, 2024. 12: p. 101875; https://doi.org/10.1016/j.rechem.2024.101875

[28] Khan, M., et al., Materials Chemistry and Physics, 2022. 274: p. 125177; https://doi.org/10.1016/j.matchemphys.2021.125177

[29] Khan, M., et al., Materials Research Express, 2019, 12(6): p. 126420; https://doi.org/10.1088/2053-1591/ab58d5

[30] Hasan, M., et al., Journal of the American Ceramic Society, 2024. p. 20329; https://doi.org/10.1111/jace.20329